UNIVERSITÀ POLITECNICA DELLE MARCHE
Repository ISTITUZIONALE

Optimization of the photoelastic conoscopic fringe pattern processing for the stress measurement on uniaxial PWO crystal cut parallel to the a-c plane and with variable thickness

This is a pre print version of the following article:

Original
Optimization of the photoelastic conoscopic fringe pattern processing for the stress measurement on uniaxial PWO crystal cut parallel to the a-c plane and with variable thickness / Natali, P. P.; Francesca, Cherubini; Davi', Fabrizio; Montalto, L.; Rinaldi, Daniele. - In: JOURNAL OF INSTRUMENTATION. - ISSN 1748-0221. - ELETTRONICO. - 17:(2022). [10.1088/1748-0221/17/02/P02021]

Availability:
This version is available at: 11566/294521 since: 2025-11-18T12:24:42Z

Publisher:

Published
DOI:10.1088/1748-0221/17/02/P02021

Terms of use:

The terms and conditions for the reuse of this version of the manuscript are specified in the publishing policy. The use of copyrighted works requires the consent of the rights' holder (author or publisher). Works made available under a Creative Commons license or a Publisher's custom-made license can be used according to the terms and conditions contained therein. See editor's website for further information and terms and conditions.
This item was downloaded from IRIS Università Politecnica delle Marche (https://iris.univpm.it). When citing, please refer to the published version.

(Article begins on next page)

23 April 2026

Optimization of the photoelastic conoscopic fringe pattern processing for the stress measurement on uniaxial PWO crystal cut parallel to the a-c plane and with variable thickness.

P.P. Natali, [1,4,*] F.Cherubini,[1,4] F. Davì,[1,4,5] L. Montalto,[2,4] D. Rinaldi.[3,4]

1- DICEA, Univ. Politecnica delle Marche, Ancona (I).

2- DIISM, Univ. Politecnica delle Marche, Ancona (I).

3- SIMAU, Univ. Politecnica delle Marche, Ancona (I).

4- ICRYS, Univ. Politecnica delle Marche, Ancona (I).

F. Davì is on leave at IMT-School for Advanced Studies, Lucca, (I).

(*) Corresponding author: p.p.natali@staff.univpm.it

Abstract

This paper presents a case study in which conoscopic, non-invasive, photoelastic techniques and the associated model are applied for the first time to investigate the internal stress state of the $PbWO_4$ (PWO) uniaxial crystal, cut normal to the crystallographic a-c plane and with non-uniform thickness.

As a matter of facts indeed, in the mass production of crystals it is rather probable to have specimen of non-constant thickness. In addition, the crystal cut, normal to the a-c plane, lead to a complex fringes structure and modeling. This can affect the fringe patterns interpretation, and in turn the interpretation of the stress state within the sample. In this paper we analyze the dependence of some model parameters on the thickness, and the relative interpretation of the fringe pattern in order to obtain a reliable measure of the stress for observations normal to the a-c plane. This procedure can speed up the crystal analysis whatever the thickness of the crystal is.

NOT FOR DISTRIBUTION JINST_110P_1121 V2

1. Introduction

Scintillating crystals are materials that have the capacity to convert the high-energy radiation interacting with them into visible light [1], [2]. This characteristic makes them excellent sensors: they are key components in many measurement systems and diagnostic devices in fields like medicine, aerospace, security, and high-energy physics [1], [3]–[5].

In order to better exploit these properties, It is mandatory to develop more precise and accurate crystal structural quality control methods [6]: moreover, crystals, due to their own characteristics (they are both dense and brittle and many of them exhibit strong anisotropy), are very sensitive to stress, internal defects and structural problems, both in the production phase and in use [5], [7]–[10]; all these aspect can alter both functionality and durability, obtaining in both cases a poor performance or a damage of the material [5], [6].

The residual stress could be considered as an indicator of the quality of the crystal, because they could influence the crystal capacity of scintillating [10], [11]. In particular, since the stress modifies the refraction indices, they can also influence the light propagation within the crystal. Indeed the structural and mechanical properties of the crystal are related to the optical properties [6], [11]–[14].

Non-destructive measurement techniques are the best choice in this case, since they allow for the knowledge of the residual stress and whole quality state while preserving the crystal integrity [5], [9], [10], [15].

One of the photoelastic techniques in particular, the laser Conoscopy, is very effective for the sample inspection [4], [16].In this technique, the crystals are observed in polarized light and in whatever stress condition they are it is possible to observe a fringe pattern [4], [8], [10].

In recent works we developed a model (mainly focussed on the uniaxial $PbWO_4$, PWO) that allows the description of those fringe patterns as function of the stress tensor and the geometry of the crystal, to get a stress map for the crystal sample [10]

This paper proposes a step forward to the application of the model in the case in which the sample is observed in direction orthogonal to the *a-c* plane [9], [10]

NOT FOR DISTRIBUTION JINST_110P_1121 V2

In the model we assume as a leading parameter the fringe order *N*: this parameter is determined thanks to an image processing method and fringe pattern analysis, which are included in the model, and it is function of both thickness and stress state [8]–[10]. Other important parameters are the smallest mutual distances between the pair of fringes, named *Δy* e *Δz* (as explained in the next section), that are alike a function of both the thickness and the stress state [9].

In some cases, when the analyzed sample has no uniform thickness *d*, such a condition modifies the parameters *Δy* e *Δz* and *N* [9]. This situation makes difficult to asses the stress state within the sample.

By the means of the proposed model [9], it is possible to obtain, observing the crystal in a direction orthogonal to the *a-c* plane, the *Δy* and *Δz* functional dependence on the thickness *d*, for a fixed value of fringe orders *N* and of the semi-angle of the optic axes φ.

The appropriate fringe order selection can make the interpretation of the fringes easier and non-ambiguous with a consequent speed-up of the experiments and stress evaluation even for non-uniform thickness samples and complex residual stress states.

In this paper we studied the quality and stress distribution in a PWO crystal provided by INFN (Istituto Nazionale di Fisica Nucleare) Ferrara (I). The sample appears defective with a macroscopic scratch. Moreover the photoelastic study is possible only in direction normal to the *a-c* plane, but in this direction the thickness it is not constant being a function of the position.

2. Background: the Bertin surfaces

Our studies are focussed on PWO crystals but they can be extended in general to any tetragonal crystal and, with a certain care, to all the birefringent crystals. The analysis is based on the permittivity tensor ***B*** [11], [15], [17] and the notion of light rays delay due to the birefringence of crystals which is described by the iso-delay Bertin surfaces [6], [12]–[14]. In order to introduce briefly the elasto-optic model needed for our cases, we use three reference frames: one referred to the geometrical sample frame {*x,y,z*}, one to the crystallographic directions {*a=b, c*} and one intrinsic to the Bertin surfaces named {ξ, η, ζ}. In this work we can consider the physical sample frame {*x,y,z*} to be coincident with the crystal frame {*a,b,c*}

NOT FOR DISTRIBUTION JINST_110P_1121 V2

[9], [18], [19] as shown in Fig. 1, due to the tetragonal structure and considering the crystal-cut misalignment negligible. Small errors in crystal cutting will be taken into account in the model in the sequel.

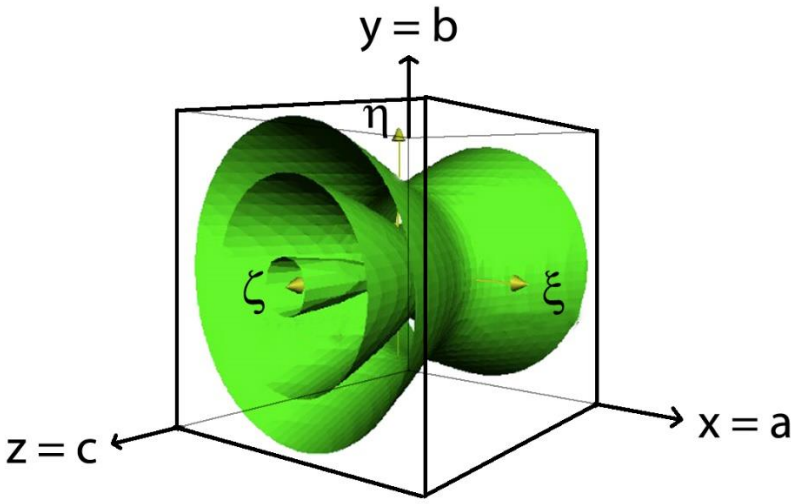

Fig. 1: Graphical representation of the three reference frames in our case of study: {*x,y,z*} referred to the geometrical sample frame, {ξ, η, ζ} intrinsic to the Bertin surfaces and the crystallographic directions {*a=b, c*}. In particular, with {ξ, η, ζ} we have the Bertin surfaces for the case of uniaxial crystal. Bertin surface for three orders N are represented in green.

The uniaxial optic axis is directed as ***c*** in case of stress-free sample, thus in our case we assume *c=z=*ζ [8], [9], [19]; the position of the axis (ξ, η) is indifferent with respect to the crystallographic directions (*a, b*), being the Bertin surfaces symmetric respect to assume *c=z=*ζ axis. An internal stress deforms the Bertin surfaces and more generally can rotate the frame (ξ, η, ζ) with respect to (*x, y, z*) [8], [9], [12].

Regarding the more specific case of PWO, it is body centred tetragonal crystal, point group 4/m with *a = b* = 0.54619 nm, *c* = 1.2049 nm (ICDD card n.19-708), where ***c*** is the uniaxial optic axis. The $\boldsymbol{\Pi}$ and $\boldsymbol{B_0}$ tensor defines the elasto-optic properties of crystal [12], [15], [17]. The piezo optic $\boldsymbol{\Pi}$ tensor, in the frame of Fig. 1, can be written as:

$$\Pi = \begin{vmatrix} \pi_{11} & \pi_{12} & \pi_{13} & 0 & 0 & \pi_{16} \\ \pi_{12} & \pi_{11} & \pi_{13} & 0 & 0 & -\pi_{16} \\ \pi_{31} & \pi_{31} & \pi_{33} & 0 & 0 & 0 \\ 0 & 0 & 0 & \pi_{44} & \pi_{145} & 0 \\ 0 & 0 & 0 & -\pi_{45} & \pi_{44} & 0 \\ \pi_{61} & -\pi_{61} & 0 & 0 & 0 & \pi_{66} \end{vmatrix} \quad (1)$$

NOT FOR DISTRIBUTION JINST_110P_1121 V2

The permittivity $\boldsymbol{B_0}$ tensor for the unstressed crystal is defined as:

$$B_0 = \begin{vmatrix} n_x^{-2} & 0 & 0 \\ 0 & n_y^{-2} & 0 \\ 0 & 0 & n_z^{-2} \end{vmatrix} = \begin{vmatrix} B_x & 0 & 0 \\ 0 & B_x & 0 \\ 0 & 0 & B_z \end{vmatrix} \quad (2)$$

Where n_x, n_y and n_z are the relative refractive indices. In the PWO tetragonal uniaxial negative crystals case we have $n_x=n_y=n_o = 2.234$ and $n_z = n_e = 2.163$, being n_o and n_e, respectively the ordinary and extraordinary indices. A residual stress, caused by a lattice distortion during the growth process, or an applied load, modifies the $\boldsymbol{B}$ tensor into:

$$\boldsymbol{B}(\boldsymbol{T}) = \boldsymbol{B}_0 + \Pi[\boldsymbol{T}], \quad (3)$$

where $\boldsymbol{T}$ is the symmetric Cauchy stress tensor.

From $\boldsymbol{B}$ is possible to calculate the eigenvalues B_i, i=1,2,3, and the corresponding eigenvectors that span the right-handed cartesian frame $\{\xi, \eta, \zeta\}$, in order to define shape and direction of the optic indicatrix [12], [15], [17]–[19] and accordingly the Bertin surfaces.

The Bertin surfaces associated to $\boldsymbol{B(T)}$ can be written in terms of the angle φ (the semi-angle of the optic axes), considering that the eigenvalues and eigenvectors of $\boldsymbol{B(T)}$ determines the angle φ and the frame $\{\xi,\eta,\zeta\}$, in the following form[6], [12], [15], [17]–[20]:

$$cos^4\varphi\xi^4 + \eta^4 + sin^4\varphi\zeta^4 + 2cos^2\varphi\xi^2\eta^2 + 2sin^2\varphi\zeta^2\eta^2 - 2sin^2\varphi cos^2\varphi\zeta^2\xi^2 - N^2H^2(\xi^2 + \eta^2 + \zeta^2) = 0 \quad (4)$$

with:

$$H = \frac{\lambda}{n_e - n_o} \quad (5)$$

Where N is an integer number that represent the fringe order and λ is the light wavelength of the observation system.

NOT FOR DISTRIBUTION JINST_110P_1121 V2

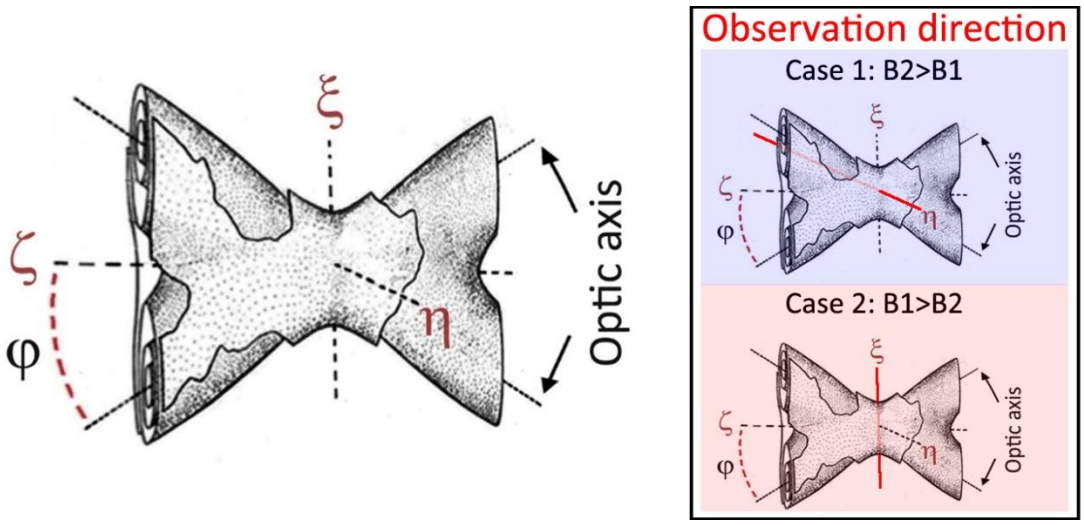

Fig. 2: Graphical representation of the reference frame {ξ, η, ζ} and the relative Bertin surfaces for the case of biaxial Crystal, where φ, named optical bisectrix, is the semi-angle between the optical axes. In the inset, are highlighted the two observation directions (red lines, that coincide with the illumination direction), studied separately in the following sections.

The equal delay surfaces named from Bertin (4) are shown in Fig.1 for the uniaxial case (φ=0) and in Fig. 2 for the biaxial case, for some *N* integer value. Depending on the crystal system, the biaxial condition surface shape can occur for a biaxial crystal or when a uniaxial crystal (that is φ=0) undergoes to a load. In the following study we consider an uniaxial crystal under a small stress state, that implies a small variation into the eigenvalues of ***B*** and small changes in the angle φ. Considering the crystal reference frames of fig.1, we can start the analysis along the *x* axis that correspond to the crystallographic direction *a* of the PWO lattice. The photoelastic technique used along *x* direction integrates the stress terms σ_{xx} τ_{xy} τ_{xz} over the specimen thickness and, being residual stress, they have zero mean value in this direction. Under such hypotheses we may safely assume that the plane stress σ_{yy}, σ_{zz}, τ_{yz} are the only measurable residual stress with this technique, and we can obtain by (1) and (2):

$$\Pi[T] = \begin{bmatrix} \sigma_{yy}\pi_{12} + \sigma_{zz}\pi_{13} & 0 & -\tau_{yz}\pi_{45} \\ \bullet & \sigma_{yy}\pi_{11} + \sigma_{zz}\pi_{13} & \tau_{yz}\pi_{44} \\ \bullet & \bullet & \sigma_{yy}\pi_{31} + \sigma_{zz}\pi_{33} \end{bmatrix} \quad (6)$$

We can assume that $|\Pi[\mathbf{T}]| << |B_{(i)}-B_{(j)}|$ or, in case of $B_{(i)}=B_{(j)}$, we assume instead $|\Pi[\mathbf{T}]| << |B(i)|$ for all the eigenvalues. In order to solve the eigenvalue problem associated with (2) and (6) we can use the Sirotin approximation [17], obtaining the following solution to within higher order terms:

NOT FOR DISTRIBUTION JINST_110P_1121 V2

$$\begin{cases} B_1 = B_x + \sigma_{yy}\pi_{12} + \sigma_{zz}\pi_{13} \\ B_2 = B_x + \sigma_{yy}\pi_{11} + \sigma_{zz}\pi_{13} \\ B_3 = B_z + \sigma_{yy}\pi_{31} + \sigma_{zz}\pi_{33} \end{cases} \quad (7)$$

Accordingly with Sirotin's results [21] the rotation of the associated principal directions is negligible in our case, furthermore for small stress the acute bisector of 2φ remains the direction determined by eigenvector B_3 [22]. Consequently, we can obtain a relation that links the angle φ to the stress:

$$sin^2\varphi(\sigma_{yy}, \sigma_{zz}) = \frac{\pm\sigma_{yy}D(\Pi)}{\Delta B + \sigma_{yy}G_{\pm}(\Pi) + \sigma_{zz}H(\Pi)} \quad (8)$$

Where $\Delta B = B_x - B_z$, $D(\Pi) = \pi_{12} - \pi_{11}$, $G_{+(\Pi)} = \pi_{12} - \pi_{31}$, $G_{-(\Pi)} = \pi_{11} - \pi_{13}$ and $H(\Pi) = \pi_{13} - \pi_{33}$.

Following [20] the angle φ is also defined as:

$$cos\varphi = \sqrt{\frac{B_{2,1} - B_3}{B_{1,2} - B_3}} \quad (9)$$

$$sin\varphi = \sqrt{\frac{B_{1,2} - B_{2,1}}{B_{1,2} - B_3}} \quad (10)$$

with the condition

$$|B_{1,2} - B_{2,1}| < |B_{1,2} - B_3| \quad (11)$$

The type of load modifies the eigenvalue ordering of ***B***, that in turn influence the sign ± in (8). Taking into account that B_3 remains always the higher eigenvalue (accordingly the hypothesis of small stress), consequently, we have two different cases of study: $B_3 > B_2 > B_1$ or $B_3 > B_1 > B_2$. From (7) the two cases depend on the sign of σ_{yy} (compression, traction) [9], [14], therefore they are related to the stress direction.

In each case of study, by ordering the eigenvalues and the eigenvectors, a univocal description of the Bertin surfaces and the angle φ in the frame {ξ,η,ζ} is given.

NOT FOR DISTRIBUTION JINST_110P_1121 V2

3. Description and analysis of the fringe orders.

As analysed in the following section, in one case the observation direction is parallel to the optic plane ($B_2 > B_1$), in the other case with ($B_1 > B_2$), the observation is carried out orthogonally to the optic plane.

3.1. Case B_2>B_1

When $B_2 > B_1$ the crystallographic frame {*x, y, z*} coincides with the frame intrinsic to the Bertin surfaces (Fig.1) and the optic angle lies in the plane (*x, z*) ≡ (ξ, ζ). Following [9], in order to get the interference fringes as a section of the Bertin surfaces with the observation plane normal to ξ ≡ *x* ≡ *d*, were *d* is the sample thickness, we set this relation inside the Bertin equation in the frame {*x,y,z*}, obtaining:

$$y^4 + z^4(sin^4\varphi) + y^2(2cos^2\varphi d^2 - N^2H^2) + z^2(-2sin^2\varphi cos^2\varphi d^2 - N^2H^2) + z^2y^2(2sin^2\varphi) + cos^4\varphi d^4 - N^2H^2d^2 = 0 \qquad (12)$$

Starting from the (12) it is possible to represent two families of interference fringes considering different values of the fringe order *N* and a fixed value for the sample thickness (Fig.3). From [9] it is possible to obtain the relation which discretizes the two families:

$$\widehat{N} = \frac{cos^2\varphi d}{H} \qquad (13)$$

With $\lfloor\widehat{N}\rfloor$ and previous fringe orders it is possible to represent the first family of interference fringes, that are symmetrical respect to the *y* axis. The fringe order $\lfloor\widehat{N}\rfloor$ generates the lowest measurable distance *Δz* described by (14)[9], and the previous fringe orders present a gradually increasing of this distance (Fig.3a).

$$\Delta z(\varphi) = \frac{\sqrt{2}\lfloor\widehat{N}\rfloor H}{sin^2\varphi}\sqrt{2sin^2\varphi cos^2\varphi K^2 + 1 - \sqrt{1 + 4sen^2\varphi K^2}} \qquad (14)$$

where *K* is defined by:

$$K = \frac{d}{NH}. \qquad (15)$$

Conversely, with $\lceil\widehat{N}\rceil$ and subsequent fringe orders it is possible to represent the second family of the interference fringes, that are symmetrical respect to the z axis. The fringe order $\lceil\widehat{N}\rceil$ generates the lowest measurable distance *Δy* represented by (16)[9], and the subsequent fringe orders present a gradually increasing of this distance (Fig.3b).

NOT FOR DISTRIBUTION JINST_110P_1121 V2

$$\Delta y(\varphi) = \sqrt{2}\lceil \hat{N} \rceil H \sqrt{1 - 2cos^2\varphi K^2 + \sqrt{1 + 4sen^2\varphi K^2}} \quad (16)$$

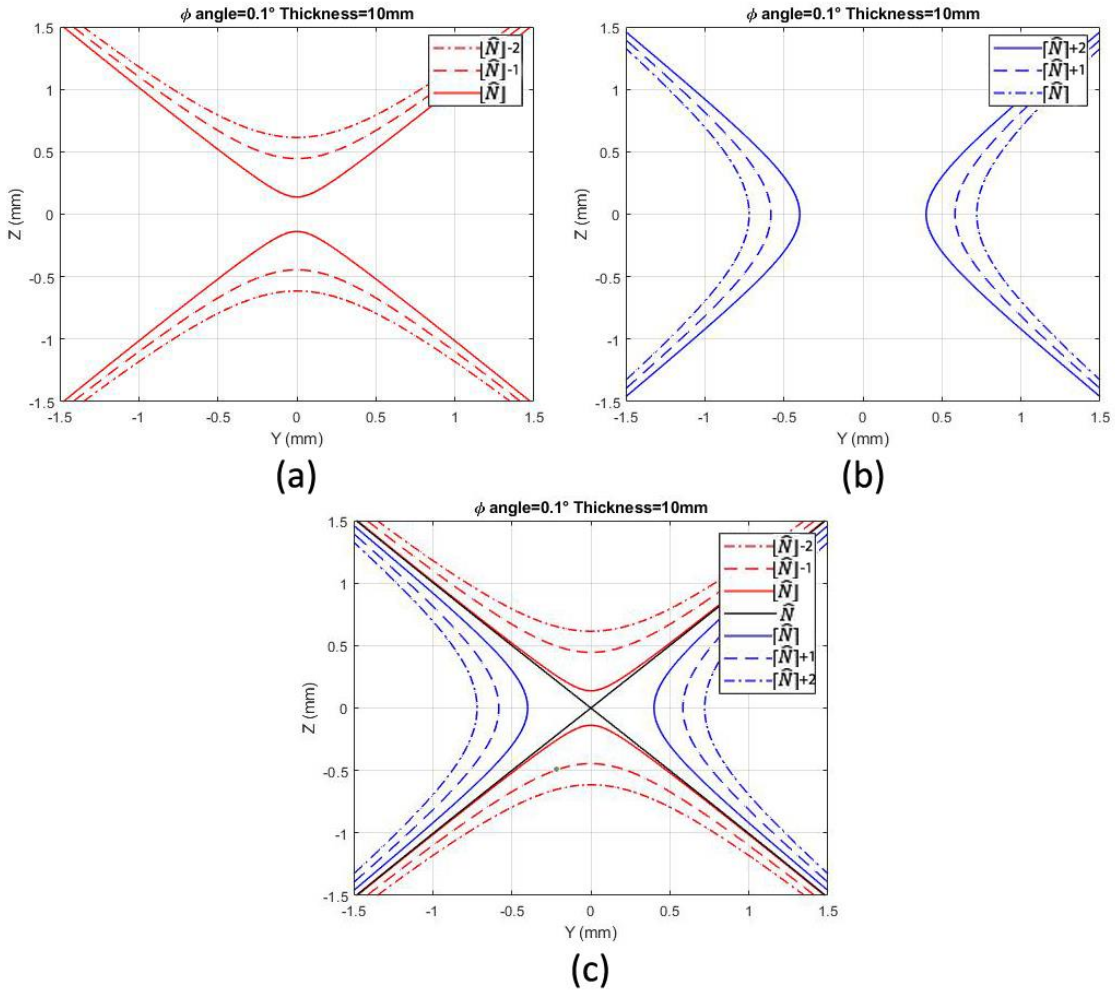

Fig. 3: Graphical representation of the two distinct families of interference fringes. In a) we have the family of fringes that are symmetrical respect to the Y axis, produced for the fringe order $\lceil \hat{N} \rceil$ and the previous integer values. This fringes produces each one a distance ΔZ between the two fringe branches, that increase its value for decreasing fringe orders. In b) we have the other possible family of interference fringes symmetrical respect to the Z axis, produced for the fringe order $\lceil \hat{N} \rceil$ and subsequent integer values. That fringes instead produces a distance ΔY that is minimal for the fringe order $\lceil \hat{N} \rceil$ and increase its value for the subsequent fringe orders. In c) we have a overall representation of the whole fringe pattern composed by the two families of interference fringes, with superimposed the parameter $\hat{N}$ that represent the separation condition between the two families of interference fringes. This parameter, graphed as a fringe order, represent the collapse condition of both parameter ΔZ and ΔY.

Once fixed the *d* parameter that represent the sample thickness, in the equations (14) and (16) the unique variable is defined by the φ angle that, from (8) is a function of the stress state. From [9], in order to have a faster and reliable algorithm for a stress state description with only one parameter, is introduced the quantity:

$$R(\sigma_{yy}, \sigma_{zz}) = (\Delta z/\Delta y)^2 \quad (17)$$

NOT FOR DISTRIBUTION JINST_110P_1121 V2

Graphing *Δy*, *Δz* and *R* as a function of the φ angle it is possible to obtain the correlation between the measuring parameter and the stress magnitude [9]. Considering for instance *d*=10mm and variation of φ from 0 to 0.5 degrees we obtain the graphs on Fig. 4.

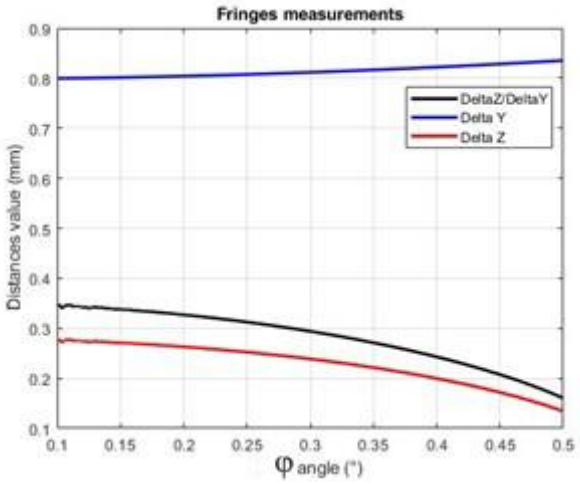

Fig. 4: Numerical simulation of the parameters *Δy*, *Δz* and *Δy/Δz* graphed in function of the φ angle variation. For this example, are considered as model parameter a thickness *d*=10mm and a φ variation from 0 to 0.5 degrees.

On the other hand, it is easily possible to find samples with also important non-homogeneity of the thickness. From (14) and (16) a *d* variation modifies the *Δy* and *Δz* parameters, and from (13) modifies the $\widehat{N}$ parameter. A significant variation of $\widehat{N}$ modify the separation between the two family of interference fringes, making necessary to use a different fringe order for the *Δy* and *Δz* estimation. In the following we will analyze the contribution of thickness assuming a variation of *d* from 8.994 to 9.000mm. This particular variation has been considered in relation to the geometrical condition of the sample analyzed in section 4, which has 9 mm as nominal value of thickness but also a surface inclination which leads to a calculated value of 8.994 mm on the opposite edge of the sample. For a fixed φ angle of 0.1 degree we can obtain the following fringes variation for *Δy* (Fig. 5) and *Δz* (Fig. 6) parameters.

NOT FOR DISTRIBUTION JINST_110P_1121 V2

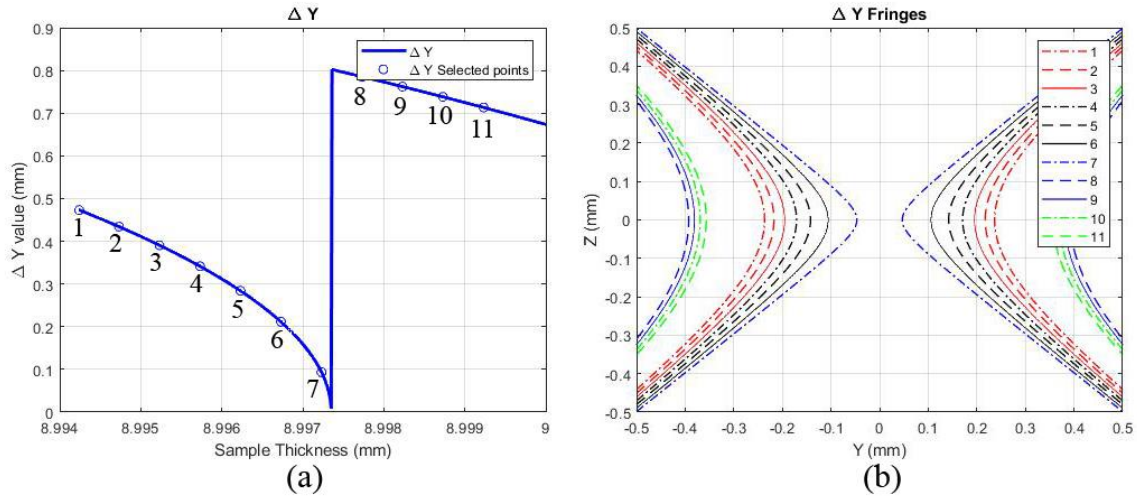

Fig. 5: Effect of the thickness variation on the *Δy* parameter for a fixed value of the φ angle. In a) we have imposed the thickness variation from 8.994mm to 9.000mm for a fixed value of φ equal to 0.1 degrees, in order to obtain the graph that correlates the thickness variation with the *Δy* parameter value. It is important to remark that the graph present a point of discontinuity that make difficult to understand the correlation between the two parameters. In b) we have graphed a representation of a series of fringes related to the correspondents numbered point in a). It is important to underline that from the points 7 and 8 there is a discontinuity due to the fringe order variation in the model.

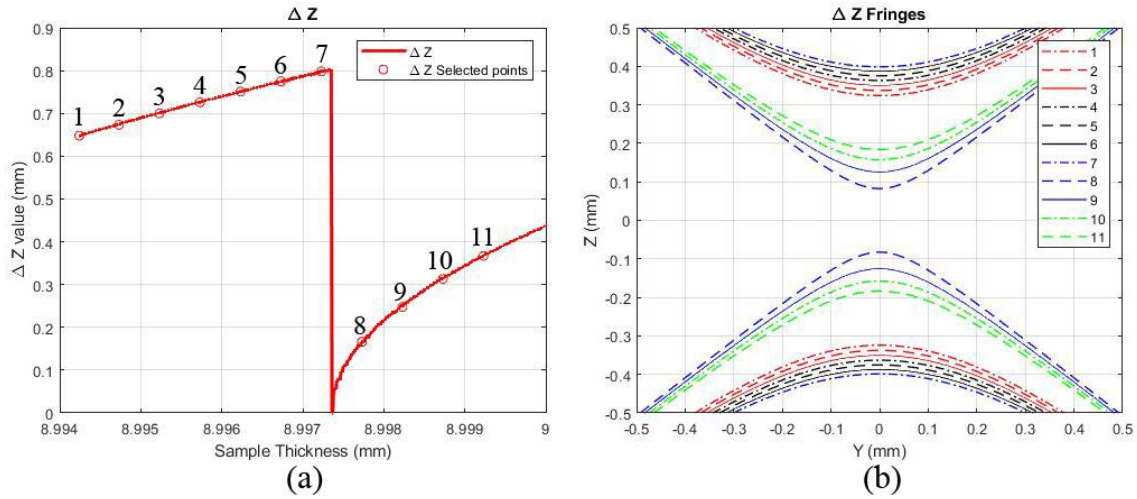

Fig. 6: Numerical simulation of the correlation between the Δz parameter and the thickness variation for a fixed value of the φ angle. In a) we have selected a fixed value of φ equal to 0.1 degree and a thickness variation from 8.994mm to 9.000mm, obtaining the correlation between the thickness variation and the Δz parameter on the graph. It is important to note the discontinuity point that make ambiguous the correlation between the two parameters. In b) we have graphed a representation of a series of fringes related to the correspondents numbered point in a). It is important to underline that from the points 7 and 8 there is a discontinuity due to the fringe order variation in the model.

The discontinuity condition on both the graphs of fig. 5a and 6a are caused by a variation of the $\widehat{N}$ (depending on the thickness) parameter such as to modify the values of $\lfloor \widehat{N} \rfloor$ and $\lceil \widehat{N} \rceil$ in the simulation. The transition between two fringe orders is represented by the collapse of *Δy* and *Δz* (Fig. 7).

NOT FOR DISTRIBUTION JINST_110P_1121 V2

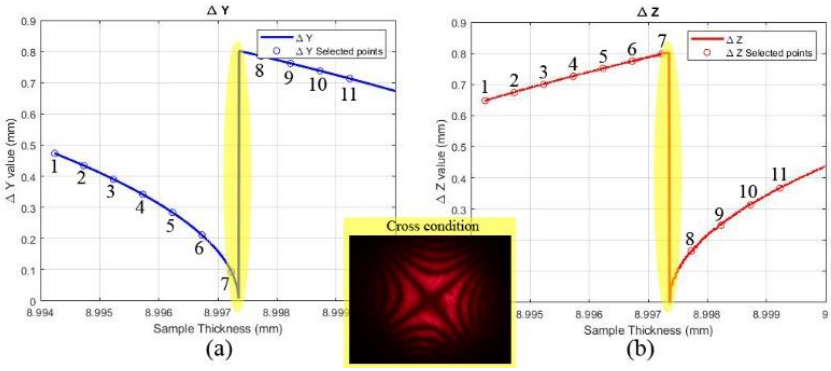

Fig. 7: We have underlined the discontinuity condition on both the graphs for Δy (a) and Δz (b). This condition is justified by the occurrence of the cross condition for a certain combination of sample thickness and φ. This circumstance correspond to the simultaneous collapse of Δy and Δz parameters, easy to be observed in experimental condition.

The effect of this kind of thickness variation is difficult to be removed in a sample with also a variation of φ angle. In order to overcome this problem is possible to use two fringe orders values for *Δy* and *Δz* that are chosen in a different way from the traditional one described above. We start considering that we have a linear variation of the sample thickness from the lower value (d_{min}=8.994mm) to the higher (d_{max}=9.000mm). Therefore, for *Δz* we calculate the fringe order $\lfloor \widehat{N} \rfloor$ obtained using the lowest value of the thickness (d_{min}) inside (13) and for *Δy* the fringe order $\lceil \widehat{N} \rceil$ obtained using the highest value of the thickness (d_{max}) in (13). Following this consideration, in the case of Fig.5 and Fig.6, we have for *Δy* the fringe order 1007 and for *Δz* the fringe order 1005. It is now possible to obtain the *Δy* and *Δz* trend as a function of the thickness *d* parameter for the new fixed value of fringe orders (1005 and 1007) and φ (Fig.8).In brief, we choose a fringe order that ensures the absence of collapse (the cross shape) in every point of the sample along the measurement path. This technique allows to eliminate the discontinuity of *Δy* and *Δz* permitting an easier stress calculation.

NOT FOR DISTRIBUTION JINST_110P_1121 v2

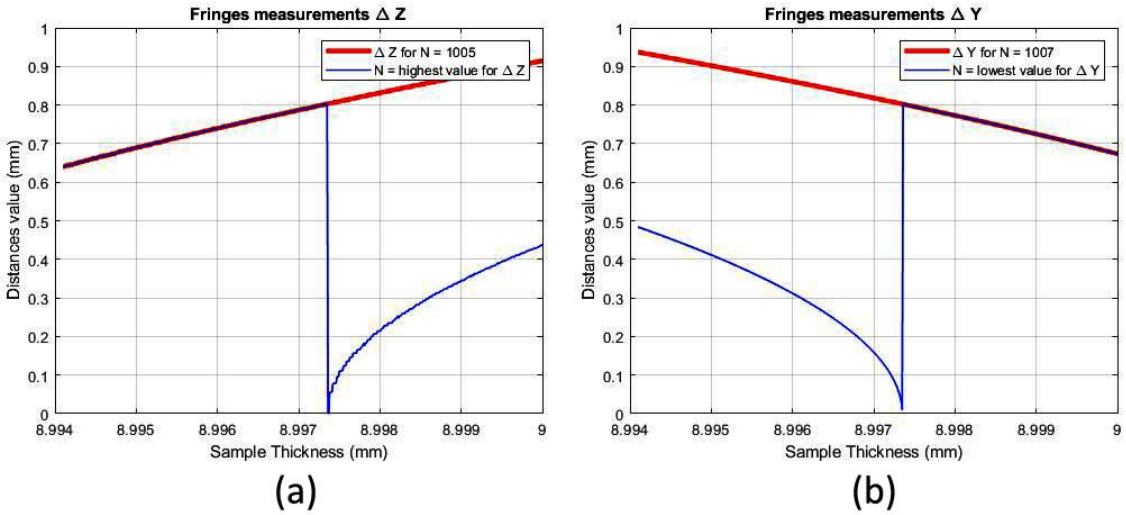

Fig. 8: For a fixed angle φ=0.1 degree in a) we have the Δz variation as a function of the sample thickness. With the blue line we have the trend obtained using the classical method, compared with the new analysis technique for a fixed fringe order N = 1005 in red. This fringe order is the last possible for *Δz* which does not produce discontinuity conditions. In b) we have the comparison between the *Δy* parameter obtained with the classical method (blue line), with the innovative method calculated using a fixed fringe order N = 1007 in red. This fringe order is the first for *Δy* which does not produce discontinuity conditions.

Using the obtained *Δy* and *Δz* values, from (17) it is possible to calculate the *R* parameter (Fig. 9).

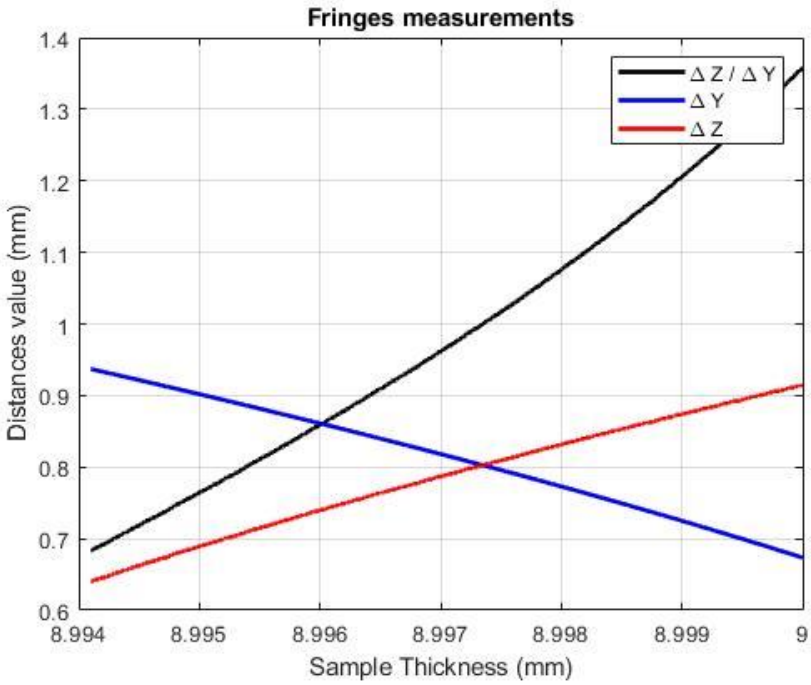

Fig. 9: Representation of the *Δy*, *Δz* and *Δy*/*Δz* parameters in function of the sample thickness, for a fixed value of φ equal to 0.1 degree. The graphs are obtained using the new analysis method that use for *Δz* the last possible fringe order which does not produce discontinuity conditions, and for *Δy* the first possible fringe order which does not produce discontinuity conditions.

NOT FOR DISTRIBUTION JINST_110P_1121 V2

The behaviour of *the ratio Δz/Δy* appears almost linear and therefore in a sample with a variation of both thickness and angle φ, it appear easy to remove the effect of *d* on the *Δy* and *Δz* parameters in (14) and (16).

3.2. Case B_1>B_2

Going back to the eigenvalue solution, we study the case when $B_1 > B_2$. The optic angle always defined in the plane (ξ, ζ) in the intrinsic frame, differently with respect to the previous case, is located on the crystallographic plane (*y, z*). Therefore, the two frames {ξ, η, ζ} and {*x, y, z*} have the ζ=*z*, but the optic plane rotates of $\frac{\pi}{2}$ about the common axis *z*. In this condition the two interference family fringes represented in Fig.3 are discretized by [9]:

$$\widehat{N} = \frac{d}{H} \tag{19}$$

As in the previous case, considering $\lfloor \widehat{N} \rfloor$ and $\lfloor \widehat{N} \rfloor$ we have the interference fringe that describe the smallest *Δz* and *Δy* distances given by the equation [9]:

$$\Delta z = \frac{\sqrt{2}\lfloor \widehat{N} \rfloor H}{sin^2\varphi} \sqrt{1 - 2sin^2\varphi K^2 - \sqrt{1 + 4sen^4\varphi K^2 - 4sen^2\varphi K^2}} \tag{20}$$

$$\Delta y = \frac{\sqrt{2}\lfloor \widehat{N} \rfloor H}{cos^2\varphi} \sqrt{1 - 2cos^2\varphi K^2 + \sqrt{1 + 4sen^4\varphi K^2 - 4sen^2\varphi K^2}} \tag{21}$$

NOT FOR DISTRIBUTION JINST_110P_1121 V2

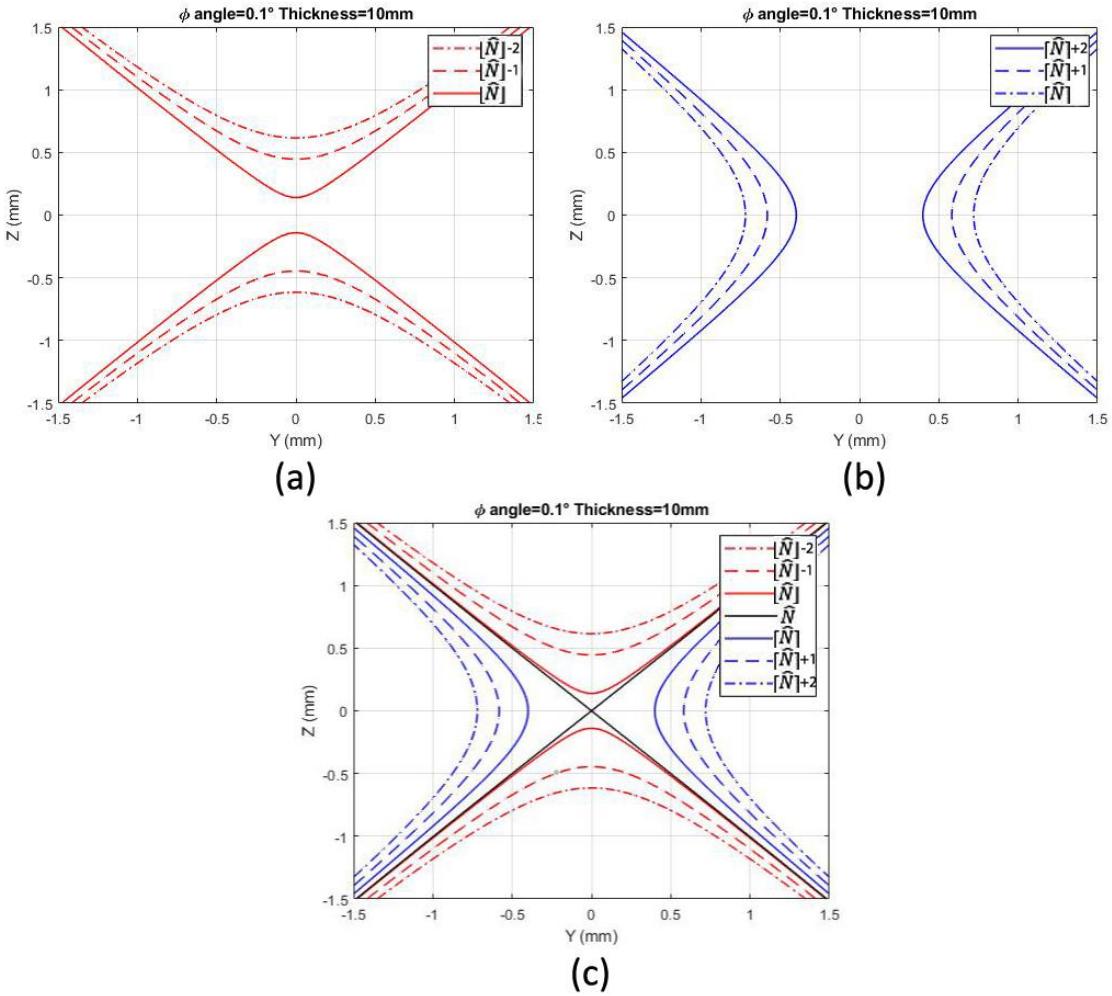

Fig. 10

Case B_1>B_2. a) family of fringes symmetrical respect to the Y axis, This fringes produces each one a distance ΔZ between the two fringe branches, that increase its value for decreasing fringe orders. In b) interference fringes symmetrical respect to the Z axis, produced for the fringe order $\lceil\widehat{N}\rceil$ and subsequent integer values. That fringes instead produces a distance ΔY that is minimal for the fringe order $\lceil\widehat{N}\rceil$ and increase its value for the subsequent fringe orders. In c) we have a overall representation of the whole fringe pattern composed by the two families of interference fringes, with superimposed the parameter $\widehat{N}$ that represent the separation condition between the two families of interference fringes. This parameter, graphed as a fringe order, represent the collapse condition of both parameter ΔZ and ΔY.

Considering *e.g.* *d*=10mm and a φ variation from 0 to 0.5 degrees we obtain the graphs on Fig. 11.

NOT FOR DISTRIBUTION JINST_110P_1121 v2

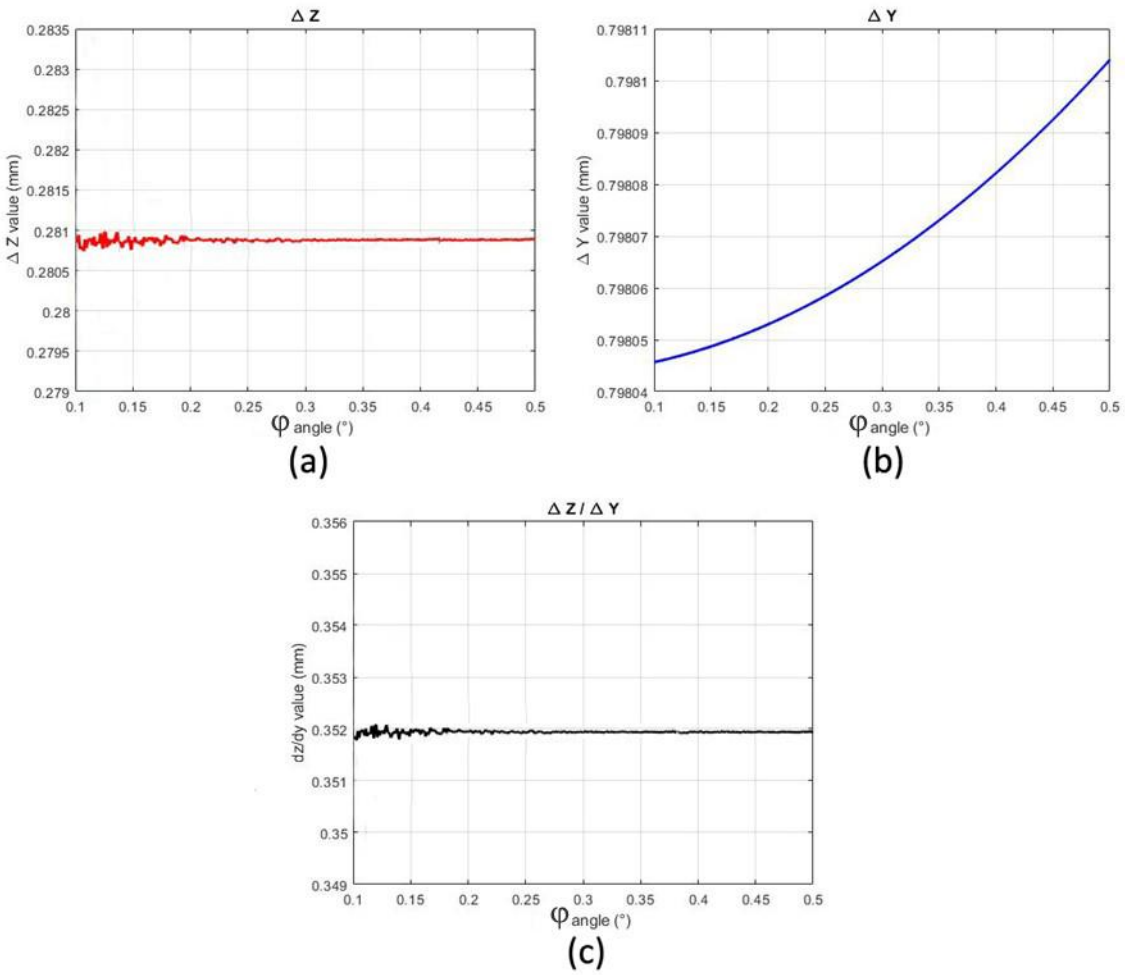

Fig. 11: Numerical simulation of the Δz parameter (a), Δy parameter (b) and Δz/Δy parameter evaluated as a function of the φ angle variation.

As in the previous case, it is important to study the presence of thickness non homogeneity. Considering the equations (19) (20) and (21), we have a dependence with the *d* parameter, therefore the behavior is similar to the previous case of study. In fact, assuming the same variation of thickness (from 8.994mm to 9.000mm) for a fixed φ angle of 0.1 degree we can obtain the fringes variation as follow for *Δy* (Fig. 12) and *Δz* (Fig. 13) parameters [9].

NOT FOR DISTRIBUTION JINST_110P_1121 v2

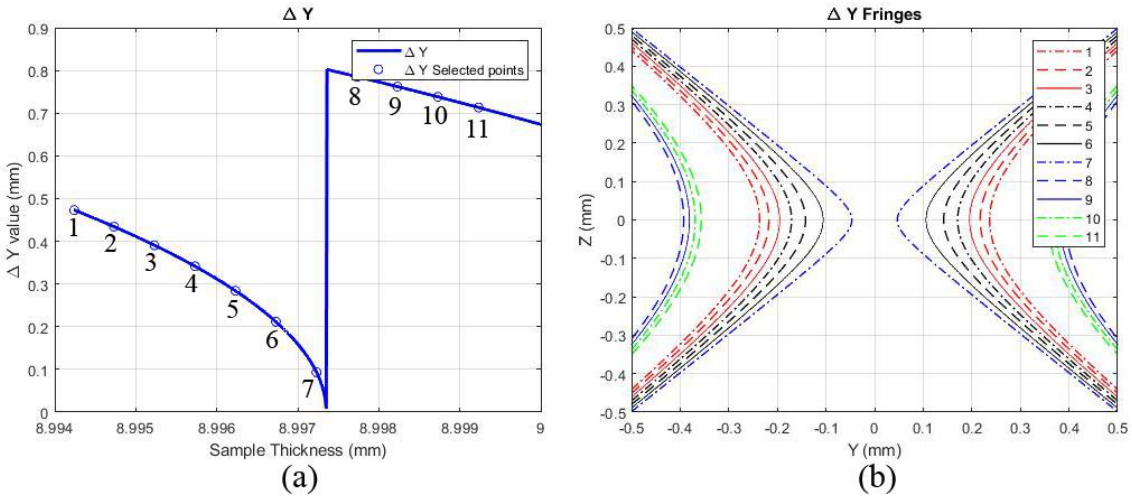

Fig. 12: Numerical evaluation of the *Δy* parameter for a fixed value of the φ angle and a thickness variation. In a) we have a thickness variation from 8.994mm to 9.000mm φ equal to 0.1 degree, in order to obtain the correlation of the thickness variation with the *Δy* parameter value. It is important to remark that the graph present a point of discontinuity. In b) we have graphed a representation of a series of fringes related to the correspondents numbered point in a). It is important to underline that from the points 7 and 8 there is a discontinuity due to the fringe order variation in the model.

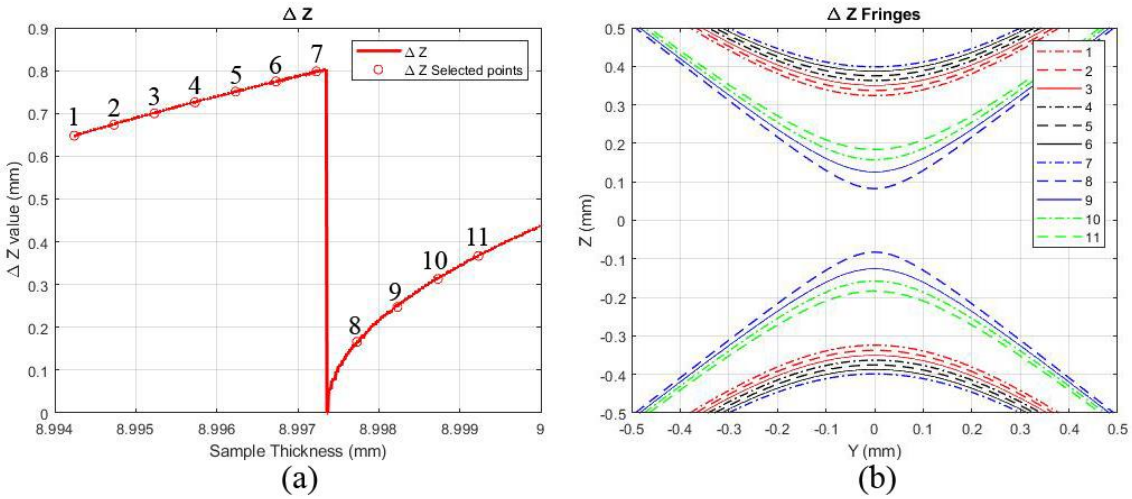

Fig. 13: Correlation evaluation between the Δz parameter and the thickness variation, utilizing a fixed value of the φ angle. In a) we have φ equal to 0.1 degree and a thickness variation from 8.994mm to 9.000mm, obtaining the correlation between the thickness variation and the Δz parameter on the graph. It is important to note the discontinuity point. In b) we have graphed a representation of a series of fringes related to the correspondents numbered point in a). It is important to underline that from the points 7 and 8 there is a discontinuity due to the fringe order variation in the model.

The discontinuity condition of both graphs (Fig. 12, Fig. 13) caused by a variation of the $\widehat{N}$ parameter, as a function of *d*, such as to modify the values of $\lfloor \widehat{N} \rfloor$ and $\lceil \widehat{N} \rceil$ can be overcome by considering for *Δz* the fringe order $\lfloor \widehat{N} \rfloor$ obtained using the lowest value of the thickness *d* inside (20) and for *Δy* the fringe order $\lceil \widehat{N} \rceil$ obtained using the highest value of the thickness *d* in (21), as we made in the previous case. Therefore, it is possible to obtain the *Δy* and *Δz*

NOT FOR DISTRIBUTION JINST_110P_1121 v2

trends as a function of the thickness *d* parameter for a fixed value of fringe orders (1005 – 1007 for Δz and Δy respectively) and φ (Fig.14).

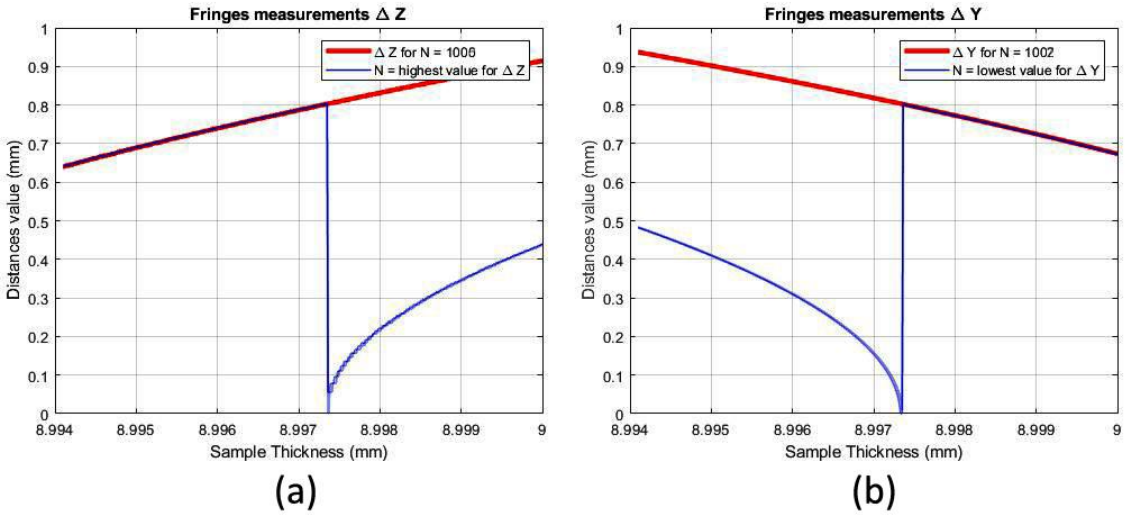

Fig. 14 Imposing a fixed value for the angle φ=0.1° in a) we have the Δz variation as a function of the sample thickness. The blue graph represents the trend obtained using the classical method, compared with the new analysis technique for a fixed fringe order N = 1005 in red. This fringe order is the nearest to the previous one that for *Δz* does not produce discontinuity conditions. In b) we have compared the *Δy* parameter obtained using the classical method in blue graph, with the innovative method calculated using a fixed fringe order N = 1007 in red. This fringe does not produce discontinuity conditions.

With the obtained values for *Δy* and *Δz*, from (17) it is possible to calculate the *R* parameter as in Fig. 15.

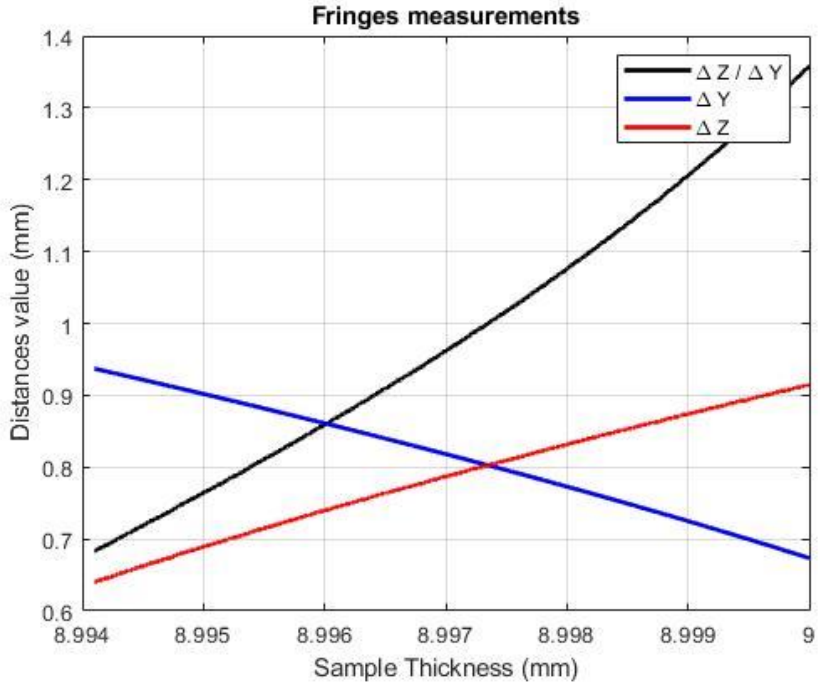

Fig. 15: Representation, using a fixed value of φ equal to 0.1°, of the *Δy*, *Δz* and *Δy*/*Δz* parameters in function of the sample thickness. The graphs are obtained using the new analysis method that use for *Δz* the last possible fringe order

NOT FOR DISTRIBUTION JINST_110P_1121 V2

which does not produce discontinuity conditions, and for *Δy* the first possible fringe order which does not produce discontinuity conditions.

Also in this case the behaviour of *Δz*/*Δy* appears almost linear, therefore the component of *d* that influences the *Δy* and *Δz* parameters in (20) and (21) appear easy to be removed.

4. Laser conoscopy fringe modelling

In this section we show the observations by means of photoelasticity, in direction normal to the ***a*-*c*** plane, of a sample with variable thickness. When we observe a sample by using laser light conoscopy [23] in direction orthogonal to the *a*-*c* plane [8][9] it is possible to obtain a fringe pattern as the one in fig. 16.

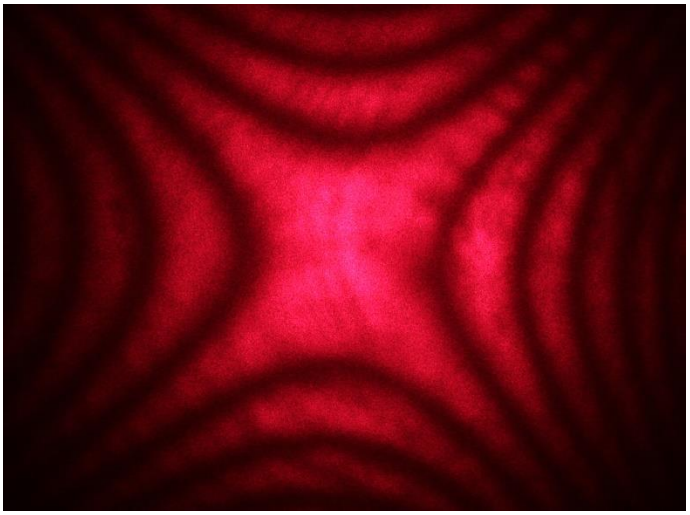

Fig. 16: Example of fringe pattern obtained with laser conoscopy in direction orthogonal to the *a*-*c* plane**. This pattern can be viewed as a section between the Bertin surface with a plane orthogonal to the ξ or η axis in the Bertin reference frame.**

Once detected the orientation of the ζ axis it is possible to evaluate the two distances *Δy* and *Δz* (Fig. 17).

NOT FOR DISTRIBUTION JINST_110P_1121 V2

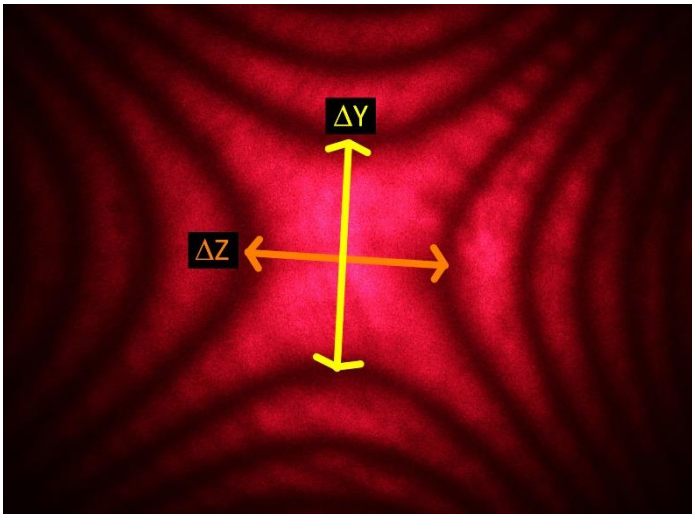

Fig. 17: Representation of the parameters Δy and Δz obtained as the smallest distance between the fringes branches, used as starting point for the punctual stress calculation and quality detection.

Using this technique is possible to scan a specified direction of the crystal in order to assess the stress distribution, that can be obtained by the *Δy* and *Δz* trends along the scan direction [8]. The weakness of this fringe analysis system is represented by the two measuring parameters *Δy* and *Δz* that are function of the stress distribution but also of the thickness sample variation (eq. (14) (16) (20) (21)).

We consider a crystal sample with 9 mm nominal thickness and the surface inclination of 0.1510 deg and 0.0110 deg on the two projections (Fig.18). The sample has been provided by INFN (Italian National Research Centre for Nuclear Physics, section of Ferrara) laboratories, which have measured the structural and geometrical condition of the sample.

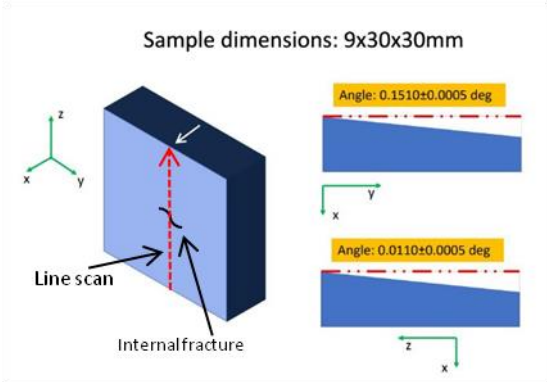

Fig. 18: Geometrical characteristics of the sample in exam, with the indication of the rough position of the internal fracture and the scanning line used for the conoscopic acquisitions. The thickness d is along the x.

The specimen presented a small internal fracture about in the middle of its volume; we concentrated our measurement and analysis on that area, scanning a line along the z direction

NOT FOR DISTRIBUTION JINST_110P_1121 V2

(see Fig. 18) crossing the internal fracture (in the range 0-26 mm starting from the sample edge see Fig. 25). A series of points on that line have been acquired via Laser Conoscopy with a step of 1mm on the crystal. A 0.064% thickness variation (from 8.952 to 8.958mm)has been assumed, considering the surface's angle of misalignment and the comparison with the simulated values. By this the measurements of the *Δy* and *Δz* values along the line have been carried out (Fig. 19).

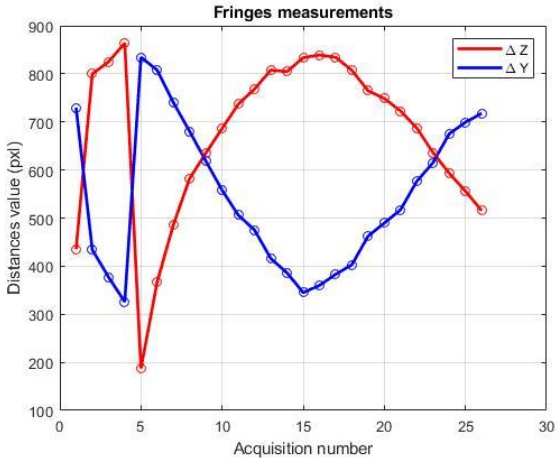

Fig. 19: Distribution of the Δy and Δz values along the scanning direction performed with laser light conoscopy carried out in direction from the lowest value of sample thickness to the highest. For each numbered punctual acquisition along the scanning direction the Δy and Δz parameters are valued. It is important to remark the presence of a discontinuity point that interrupt the graphs regularity.

Accordingly with the numerical simulations represented in Fig.5, 6, 12, 13 on the section above, the trends of each measuring parameter are strongly influenced by the thickness variation, which modifies the slope of the curves and introduces discontinuity points (Fig. 18). Therefore, as explained in the previous paragraph, it is problematic to evaluate the thickness and the φ angle variation contribution on the *Δy* and *Δz* measuring parameter, making difficult to study the parameter *R* due to its discontinuity (17). These weaknesses on the data analysis and interpretation are due to the original model that is based on the assumption of constant thickness [8], [9]. In order to generalize the data analysis, it is important to make the measurements obtained from a sample with thickness variation easily interpretable. This can be achieved through an analysis that regards the choice of the fringe to be analyzed avoiding the fringe discontinuity due to the sample thickness variation. Some considerations about the fringe choice are mandatory (following the observations made in the previous paragraph): instead of using the first visible fringe for *Δy* and *Δz* [9] as in Fig. 17, once performed a scan

NOT FOR DISTRIBUTION JINST_110P_1121 V2

as in Fig. 18, we have to count the number of discontinuities on the graphs for *Δy* or *Δz.* In our case we have one case, generated by the collapse of the *Δy* and *Δz* parameters as in fig. 20.

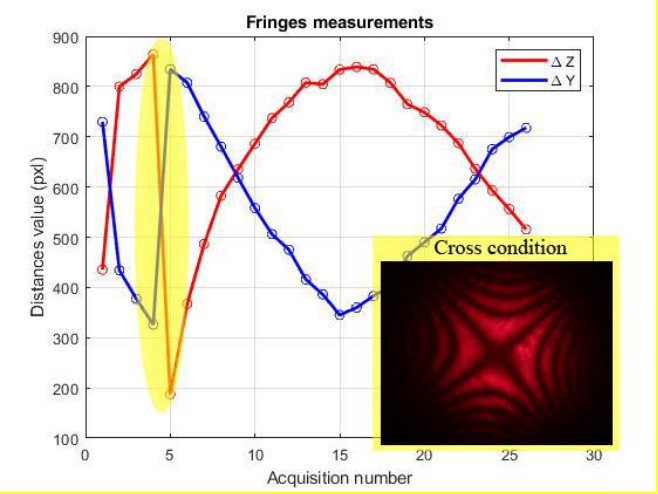

Fig. 20: Focus (in yellow) on the Δy and Δz values along the scanning direction, regarding the critical point. This condition corresponds to the collapse (the inset) of both distances Δy and Δz, named cross condition. The occurrence of this condition leads to a variation of the fringe orders considered for the analysis.

Therefore, we have to start our considerations from the first image obtained by the scan of the sample, that corresponds to the acquisition in correspondence of the lowest value of thickness along the scanning direction. Differently from the traditional fringe selection method showed in Fig.17, for *Δy* we have to skip one fringe order (equal to the number of discontinuities on the Fig.20 graphs) and for *Δz* we maintain the same fringe order (in this case the two nearest curves), as described in Fig. 21.

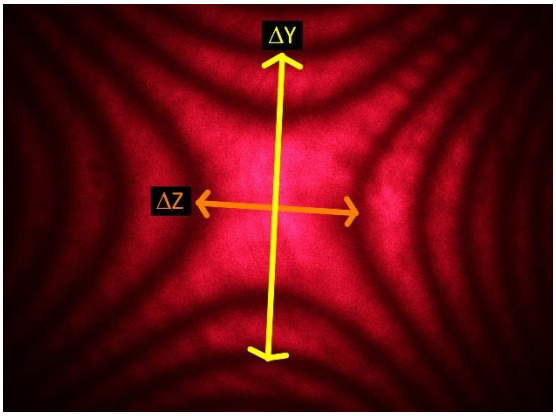

Fig. 21: Representation of the fringe orders used for the Δy and Δz evaluation. The use of this fringe orders avoid the presence discontinuity points on the Δy and Δz graph distribution along the scanning direction in the case in exam.

Now it is possible to superimpose on the *Δy* and *Δz* graphs of Fig. 19 the new graphs obtained using an unique new fringes order along the all scanning direction (Fig. 22).

NOT FOR DISTRIBUTION JINST_110P_1121 V2

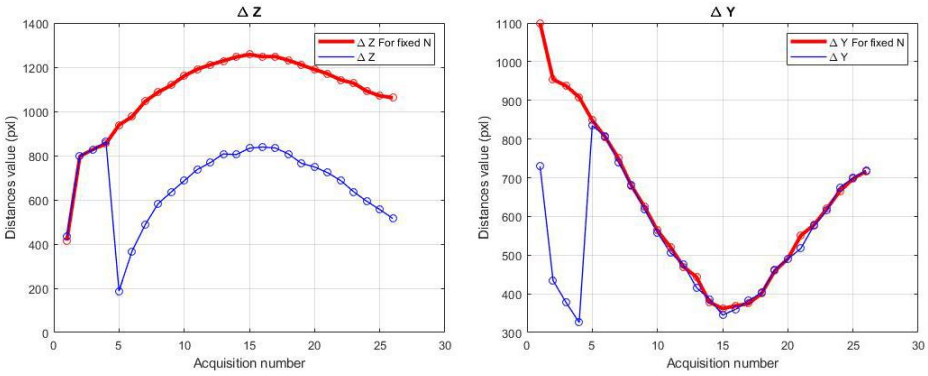

Fig. 22: Superimposition of the graphs obtained with the previous classical technique in blue, with the graphs obtained using fixed values of fringe orders in red. In a) we have this comparison for Δz, in blue are used always the smallest distance between the fringe branches along the scanning direction. In red is used, for the first acquisition, the same fringe of the blue case; but in this case we follow this fringe along the whole scanning direction, even when is available another fringe that present a smaller distance Δz. In b) we have in blue the Δy distribution obtained with the traditional analysis method and in red the results of the new technique that use a fixed fringe for Δy along the whole scanning direction. This fixed fringe is chosen starting from the fringe used in the classical method, skipping a number of fringes equal to the number of discontinuities on the Δy distribution along the scanning direction.

In general, we have to calculate the number of discontinuities on graph of *Δy* along the scanning direction, using the first visible fringes as in Fig. 17. Then, starting from the image in correspondence of the lowest value of thickness we have to jump a number of fringe orders equal to the number of discontinuities on graph of *Δy* along the scanning direction. For *Δz* we have to choose the fringe order as described previously, referring to Fig. 17. Following this two new couple of fringe along the scanning direction, is now possible to obtain a continuous graph for *Δy* and *Δz.*

This type of fringes selection perfectly fit to the model described above. In fact, we start our analysis with the image that correspond to the conoscopic acquisition for the lowest value of thickness along the scanning direction, and for *Δz* we consider the first couple of fringes. This couple of fringes corresponds, on the previous section, to the fringe order $\lceil \widehat{N} \rceil$ calculated for the lowest value of sample thickness *d.* Instead for *Δy* we consider a couple of fringes as described above, that corresponds to the fringe order $\lceil \widehat{N} \rceil$ calculated for the highest value of sample thickness *d*. Or, in our case, it corresponds to the fringe order $\lceil \widehat{N} \rceil$ calculated for the lowest value of sample thickness *d,* to which must be added an integer number equal to the number of jumps of the parameter $\lceil \widehat{N} \rceil$ from the lowest value of thickness to the highest.

NOT FOR DISTRIBUTION JINST_110P_1121 v2

As a consequence, the graphs for *Δy* and *Δz* are continuous, so it is possible to obtain the *R* parameter as in Fig. 23, as a function of the stress distribution along the scanning direction and the thickness variation

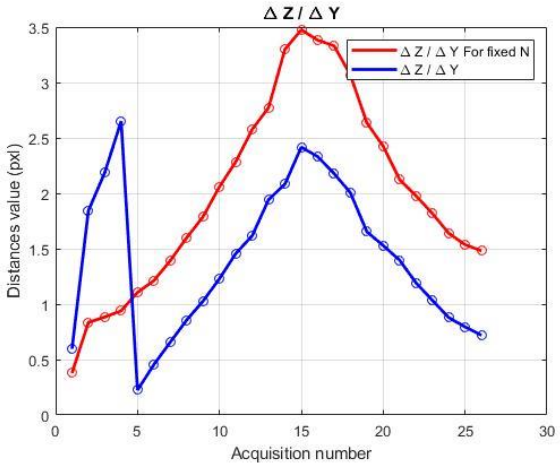

Fig. 23: Superimposition of the Δz/Δy parameter calculated using the classical analysis method in blue and with the new described method of fringe selection in red. It is worth to note the differences between the two shapes. In the red case we have no discontinuity points, therefore is easier to study the behavior of the sample along the scanning direction

4.1.**Data Analysis**

Once obtained the *R* parameter, it is possible to evaluate the stress distribution along the scanning direction. In fact, from [9], it is possible to use the linearized model that starts from the calculated $R_n = (\frac{\Delta z}{\Delta y})^2$.From this, we obtain the following relation with the stress state [9]:

$$R_n(\sigma) = R_0(K) + R_{1n}(K)(\frac{\pm(\pi_{12}-\pi_{11})}{n_x^{-2}-n_z^{-2}})\sigma_{yy} \quad (22)$$

where :

$$R_0 = K_+ \frac{\sqrt{K_-^2-1}}{\sqrt{1-K_+^2}} \quad (23)$$

and for the case $B_2>B_1$:

$$R_{11} = -2K_+^2\left[\frac{(1-K_+^2)K_-^4+(K_-^4-1)K_+^2}{(1-K_+^2)^2}\right] \quad (24)$$

whereas if $B_2<B_1$:

$$R_{12} = 2K_+^2\frac{(K_-^2-1)^2}{(1-K_+^2)} \quad (25)$$

NOT FOR DISTRIBUTION JINST_110P_1121 V2

By considering that $|\pi_{12} - \pi_{11}|$ difference is known from[19]. In our case of study we have also a thickness *d* inhomogeneity that introduces a variation of the R_0, R_{11}, and R_{12} parameters which can be evaluated once known the spatial distribution of the thickness sample value.

Considering that at our best knowledge $|\pi_{12} - \pi_{11}| = (0{,}9234 \pm 0{,}1548) \cdot 10^{-12} Pa^{-1}$, with the studied thickness variation from 8.952 to 8.958mm. Applying the model to the case $B_2 > B_1$ it is possible to obtain the graphs in Fig.2.

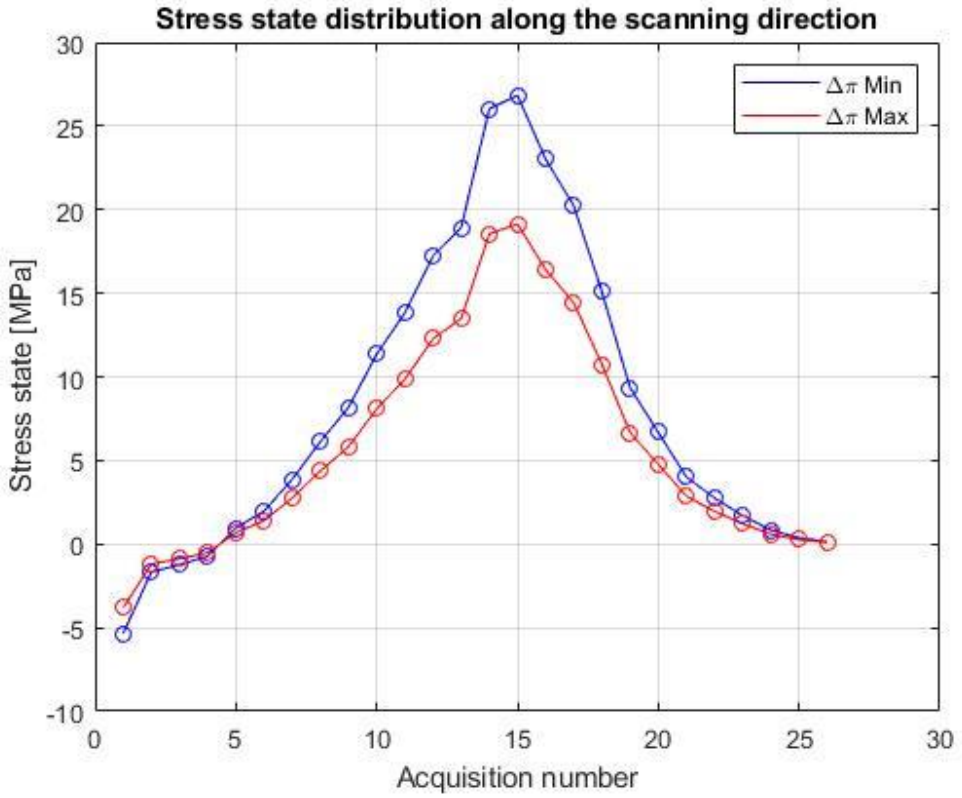

Fig. 24: Stress state distribution [MPa] along the analyzed area. The blue line denotes the results using the lowest value for the difference $|\pi_{12} - \pi_{11}|$. The red line describes the results obtained with the highest value of $|\pi_{12} - \pi_{11}|$.

The two graphs in fig 24, shows a stress peak about the sample center of 20-25 Mpa, the uncertainity in the calculation is due to the uncertainity in the difference $|\pi_{12} - \pi_{11}| = \Delta\pi$.

About the identification of the traction or tension, it depends on the sign of $\Delta\pi$, that it is still unknown at the present stage. The values obtained are close to the fracture value at the center, accordingly with the sample damage as shown in figure 25.[24]

NOT FOR DISTRIBUTION JINST_110P_1121 V2

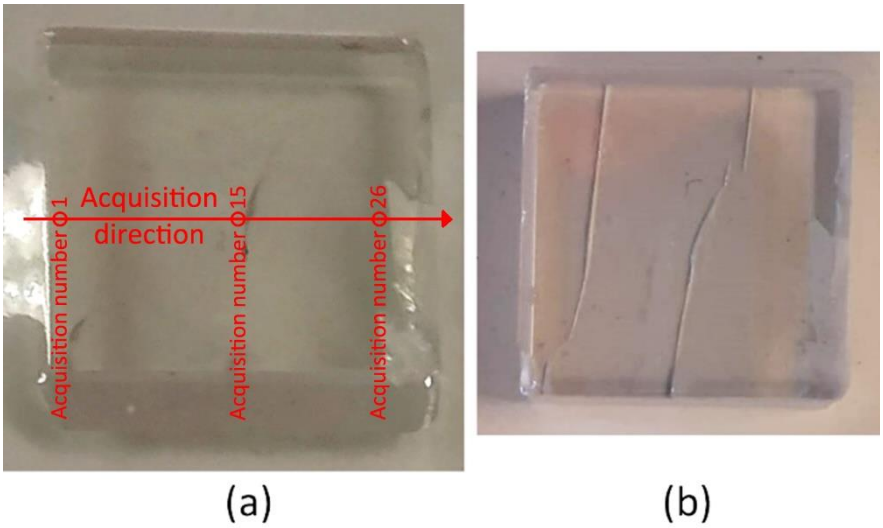

Fig. 25: a) Visible condition of the sample in exam, with the line scan indicated by the red arrow. It is important to remark that in the center of the crystal there is a damage that is not a superficial scratch but a crack. (b)This crack spread throughout the sample volume once finished the photoelastic measurements and after some months

5. Conclusions

We measured the stress distribution in PWO, observed in direction normal to the *a-c* plane, with variable sample thickness *d*. By means of the developed method is possible to remove the problems caused by an inhomogeneity of the crystal thickness in the observation, in order to extract only the stress contribution from the fringe pattern. This result is important because usually a crystal sample shows thickness variations between the surfaces. By the new technique exposed in this paper, it is possible to observe this kind of crystals in direction orthogonal to the plane *a-c* in order to study the stress distribution, without the trouble caused by the non-homogeneity of the sample geometry. This model makes possible to analyze samples that previously could not be studied with laser conoscopy due to the sample cut direction and shape. This analysis can easily be extended to other tetragonal crystals.

Acknowledgments

We wish to thank the INFN (Istituto Nazionale di Fisica Nucleare) Ferrara (I) which provided and characterized the sample, particularly Dr. Laura Bandiera, Marco Romagnoni and Andrea Mazzolari.

NOT FOR DISTRIBUTION JINST_110P_1121 v2

References

[1] P. Lecoq, "Development of new scintillators for medical applications," *Nucl. Instruments Methods Phys. Res. Sect. A Accel. Spectrometers, Detect. Assoc. Equip.*, vol. 809, pp. 130–139, Feb. 2016, doi: 10.1016/J.NIMA.2015.08.041.

[2] P. Lecoq, A. Annenkov, A. Gektin, M. Korzhik, and C. Pedrini, *Inorganic scintillators for detector systems: physical principles and crystal engineering (Particle acceleration and detection*. Springer, 2006.

[3] V. B. Brudanin, N. A. Gundorin, A. A. Filossofov, D.V. Nemtchenok, I.B. Smolnikov, S. I. Vasiliev, and V. I. Bregadze, "Element-loaded organic scintillators for neutron and neutrino physics.," *Identif. Dark Matter, Proc. 3 rd Int. Work. York, UK, 18–22 Sept. 2011*, vol. 6, pp. 6626–6634, 2011.

[4] P. P. P. Natali, L. Montalto, D. Rinaldi, F. Davi, N. Paone, and L. Scalise, "Noninvasive Inspection of Anisotropic Crystals: Innovative Photoelasticity-Based Methods," *IEEE Trans. Nucl. Sci.*, vol. 65, no. 8, pp. 2203–2207, 2018, doi: 10.1109/TNS.2018.2808702.

[5] D. Rinaldi, L. Montalto, M. Lebeau, and P. Mengucci, "Influence of a Surface Finishing Method on Light Collection Behaviour of PWO Scintillator Crystals," *Photonics*, vol. 5, 47, 2018.

[6] J. W. Dally and W. F. Riley, *Experimental Stress Analysis*. Toledo, OH, USA, 1966.

[7] L. Montalto *et al.*, "Quality control and structural assessment of anisotropic scintillating crystals," *Crystals*, vol. 9, no. 7, 2019, doi: 10.3390/cryst9070376.

[8] L. Montalto *et al.*, "Characterization of a defective PbWO 4 crystal cut along the a-c crystallographic plane: structural assessment and a novel photoelastic stress analysis," *J. Instrum.*, vol. 12, no. 12, p. P12035, 2017, [Online]. Available: http://stacks.iop.org/1748-0221/12/i=12/a=P12035.

[9] P. P. P. Natali, L. Montalto, L. Scalise, F. Davì, N. Paone, and D. Rinaldi, "Fringe modelling and photoelastic stress measurement method in tetragonal PWO observed in the plane normal to a crystallographic a-axis," *J. Instrum.*, vol. 15, no. 9, pp. P09037–P09037, 2020, doi: 10.1088/1748-0221/15/09/P09037.

NOT FOR DISTRIBUTION JINST_110P_1121 V2

[10] L. Montalto *et al.*, "Quality control and structural assessment of anisotropic scintillating crystals," *Crystals*, vol. 9, no. 7, 2019, doi: 10.3390/cryst9070376.

[11] D. Ding *et al.*, "Effects of anisotropy on structural and optical characteristics of LYSO:Ce crystal," *Phys. status solidi*, vol. 251, no. 6, pp. 1202–1211, Jun. 2014, doi: 10.1002/pssb.201350338.

[12] J. F. Nye, *Physical properties of crystals*. Clarendon Press, 1985.

[13] D. Rinaldi, P. Pietroni, and F. Davì, "Isochromate fringes simulation by Cassini-like curves for photoelastic analysis of birefringent crystals," *Nucl. Instruments Methods Phys. Res. Sect. A Accel. Spectrometers, Detect. Assoc. Equip.*, vol. 603, no. 3, pp. 294–300, 2009, doi: 10.1016/j.nima.2009.02.020.

[14] D. Rinaldi, F. Daví, and L. Montalto, "On the photoelastic constants and the Brewster law for stressed tetragonal crystals," *Math. Methods Appl. Sci.*, vol. 41, no. 8, pp. 3103–3116, 2018, doi: 10.1002/mma.4804.

[15] N. V. Perelomova and M. M. Tagieva, *Problems in crystal physics with solutions, Edited by M.P. Shaskol'skaya translated from the Russian by V.I. Kisin*. Moscow: Mir Publisher.

[16] A. Ciriaco *et al.*, "PWO photo-elastic parameter calibration by laser-based polariscope," *Nucl. Instruments Methods Phys. Res. Sect. A Accel. Spectrometers, Detect. Assoc. Equip.*, vol. 570, no. 1, pp. 55–60, 2007, doi: 10.1016/j.nima.2006.09.095.

[17] Y. I. Sirotin and M. P. Shaskolskaya, *Fundamentals of Crystal Physics*. Moscow, 1982.

[18] F. Daví and D. Rinaldi, "Mechanical and Optical Properties of Anisotropic Single-Crystal Prisms," *J. Elast.*, vol. 120, no. 2, pp. 197–224, Aug. 2015, doi: 10.1007/s10659-014-9511-4.

[19] P. P. Natali *et al.*, "Theoretical and experimental evaluation of piezo-optic parameters and photoelastic constant in tetragonal PWO," *Appl. Opt.*, vol. 57, no. 4, p. 730, 2018, doi: 10.1364/ao.57.000730.

[20] E. E. Wahlstrom, *Optical crystallography*. Wiley, 1969.

[21] F. Daví, "On the Bertin surfaces of photoelastic crystals," *J. Opt. Soc. Am. A*, vol. 32, no. 12, p. 2323, Dec. 2015, doi: 10.1364/JOSAA.32.002323.

NOT FOR DISTRIBUTION JINST_110P_1121 V2

[22] D. Rinaldi, F. Daví, and L. Montalto, “On the photoelastic constants for anisotropic stressed crystals,” *Nucl. Instruments Methods Phys. Res. Sect. A Accel. Spectrometers, Detect. Assoc. Equip.*, vol. 947, p. 162782, 2019, doi: https://doi.org/10.1016/j.nima.2019.162782.

[23] L. Montalto, N. Paone, D. Rinaldi, and L. Scalise, “Inspection of birefringent media by photoelasticity: from diffuse light polariscope to laser conoscopic technique,” *Opt. Eng.*, vol. 54, no. 8, p. 081210, 2015, doi: 10.1117/1.OE.54.8.081210.

[24] M. Ishii, K. Harada, M. Kobayashi, Y. Usuki, and T. Yazawa, “Mechanical properties of PbWO4 scintillating crystals,” *Nucl. Instruments Methods Phys. Res. Sect. A Accel. Spectrometers, Detect. Assoc. Equip.*, vol. 376, no. 2, pp. 203–207, Jul. 1996, doi: 10.1016/0168-9002(96)00247-1.

NOT FOR DISTRIBUTION JINST_110P_1121 v2

NOT FOR DISTRIBUTION JINST_110P_1121 v2